^{64}Cu-*p*-NH_2-Bn-DOTA-hu14.18K322A, a PET Radiotracer Targeting Neuroblastoma and Melanoma

Amy L. Vāvere[1], Elizabeth R. Butch[1], Jason L.J. Dearling[2], Alan B. Packard[2], Fariba Navid[3], Barry L. Shulkin[1], Raymond C. Barfield[4], and Scott E. Snyder[1]

[1]Division of Nuclear Medicine, Department of Radiological Sciences, St. Jude Children's Research Hospital, Memphis, Tennessee; [2]Division of Nuclear Medicine and Molecular Imaging, Department of Radiology, Children's Hospital Boston and Harvard Medical School, Boston, Massachusetts; [3]Department of Oncology, St. Jude Children's Research Hospital, Memphis, Tennessee; and [4]Division of Hematology-Oncology, Department of Pediatrics, Duke University Medical Center, Durham, North Carolina

The hu14.18K322A variant of the GD2-targeting antibody hu14.18 has been shown to elicit a level of antibody-dependent cell-mediated cytotoxicity toward human neuroblastoma cells similar to that of the parent antibody. However, hu14.18K322A exhibited a decreased complement activation and associated pain, the dose-limiting toxicity in neuroblastoma immunotherapy. PET with a radiolabeled analog of the same antibody used in treatment will provide insight into the ability of hu14.18K322A to reach its target, as well as nontarget uptake that may cause side effects. Such antibody radiotracers might also provide a method for measuring GD2 expression in tumors, thus enabling the prediction of response to anti-GD2 therapy for individual patients. **Methods:** The conjugation of hu14.18K322A with *p*-NH_2-Bn-DOTA was accomplished using *N*-(3-dimethylaminopropyl)-*N′*-ethylcarbodiimide with subsequent ^{64}Cu radiolabeling at 37°C for 30 min. Immunoreactivity of the conjugate was assessed by a dose-escalation blocking experiment measuring binding to purified GD2 versus GD1b as a negative control. Cell uptake and biodistribution studies in M21 (GD2-positive) and PC-3 (GD2-negative) tumor models were performed, as was small-animal PET/CT of M21 and PC-3 tumor–bearing mice. **Results:** The labeling of ^{64}Cu-*p*-NH_2-Bn-DOTA-hu14.18K322A was achieved at more than 95% radiochemical purity and a specific activity of 127–370 MBq/mg (3.4–10 mCi/mg) after chromatographic purification. Preliminary in vitro data demonstrated a greater than 6-fold selectivity of binding to GD2 versus GD1b and dose-dependent inhibition of binding by unmodified hu14.8K322A. In vivo data, including small-animal PET/CT, showed significant GD2-positive tumor-targeting ability, with a persistent 2-fold-higher uptake of radiotracer than in GD2-negative tumors. **Conclusion:** ^{64}Cu-*p*-NH_2-Bn-DOTA-hu14.18K322A represents a novel PET radiotracer to facilitate clinical investigations of anti-GD2 immunotherapies and to complement other imaging modalities in the staging and treatment of neuroblastoma.

Key Words: ^{64}Cu; neuroblastoma; disialoganglioside GD; antibody; positron emission tomography

J Nucl Med 2012; 53:1772–1778
DOI: 10.2967/jnumed.112.104208

Received Feb. 7, 2012; revision accepted Jun. 18, 2012.

For correspondence or reprints contact: Scott E. Snyder, Department of Radiological Sciences, St. Jude Children's Research Hospital, Mail Stop #220, 262 Danny Thomas Pl., Memphis, TN 38105.

E-mail: scott.snyder@stjude.org

Published online Oct. 12, 2012.

Neuroblastoma is the most common extracranial solid tumor in early childhood, with a median age at diagnosis of 15 mo (*1*). Greater than 60% of all neuroblastoma patients are categorized as high-risk on the basis of age at diagnosis, presence of disseminated disease, and histologic and genetic factors. Even with an aggressive combination of chemotherapy, surgery, and radiation, the survival rate for these patients is only approximately 30%–40% (*2,3*). Although 5-y survival rates for neuroblastoma have increased by 20% in the last 30 y, it continues to be one of the more aggressive types of childhood cancer when discovered in later stages (*4*). Intensive chemotherapy and resection achieves major regressions of stage 4 neuroblastoma, but most patients still succumb to microscopic metastases that are not responsive to therapy (*2*). In recent years, researchers have focused their efforts in neuroblastoma on immunotherapies that specifically target this microscopic residual disease (*5–13*). These antibodies target the antigen GD2 and engage natural killer cells to initiate antibody-dependent cell-mediated cytotoxicity, thereby exploiting the patient's own immune system to attack the tumor cells (*14*).

Disialoganglioside GD2 is a glycolipid expressed on cells of neuroendocrine origin and is thought to be involved in cellular adhesion to the substratum (*15*). GD2 is the major ganglioside expressed on neuroblastoma and melanoma cells and is minimally expressed in most other tissues of the body, making it an attractive target for immunotherapy (*14*). In 1985, Saito et al. examined the specificity of several antibodies to GD2, resulting in the selection of 3F8, a murine antibody, as a primary candidate (*16*). Saarinen et al. from the same group demonstrated that 3F8 was effective in eradicating neuroblastoma cells from bone marrow (*17*). Capitalizing on the effectiveness of targeting GD2 for neuroblastoma immunotherapy, Mueller et al. developed a chimeric antibody based on 14.18, another murine GD2-targeting antibody not derived from 3F8. This chimeric antibody, ch14.18, demonstrated specificity for GD2 and induction of cell-mediated lysis of neuroblastoma cells (*18,19*). Since that time, ch14.18 has shown promise through several phase I trials as a stand-alone treatment and in

conjunction with cytokines to increase the immune response, for both melanoma (*6–9*) and neuroblastoma (*10–13*).

Most recently, a study by the Children's Oncology Group demonstrated an increase of 20% in 2-y event-free survival and an increase of 10% in overall survival using a maintenance therapy of *cis*-retinoic acid and ch14.18 in conjunction with a cytokine regimen versus *cis*-retinoic acid alone (*20*). On the basis of these results, anti-GD2 immunotherapy is becoming the standard of care. However, since its introduction, dose-limiting toxicities, principally pain, have been observed. While eliciting antibody-dependent cell-mediated cytotoxicity, these antibodies also activate complement, which appears to be linked to the toxicities (*5,18,19*). To address this issue, a humanized version of ch14.18 was developed containing a single-point mutation that was shown to decrease complement activation with the goal of minimizing dose-limiting side effects (*21*). This mutant humanized antibody, hu14.18K322A, exhibits dramatically decreased complement-dependent cytotoxicity, with a significant decrease in pain after 2 h (*21*). Compared with ch14.18, this faster pain resolution did not come at the expense of any significant difference in antibody-dependent cell-mediated cytotoxicity. The decreased complement-dependent cytotoxicity induced by the point mutant not only makes the therapy much more tolerable for the pediatric patient population but also should allow an increase in maximum-tolerated dose. A phase I trial is ongoing at St. Jude Children's Research Hospital using hu14.18K322A for treating children and adolescents with neuroblastoma or melanoma (*22*).

We describe here the ^{64}Cu-labeling and preliminary biologic evaluation of ^{64}Cu-*p*-NH_2-Bn-DOTA-hu14.18K322A. The 12.7-h half-life of ^{64}Cu enables PET at the late time points needed for localization of the full-length antibody. The chimeric GD2 antibody was successfully labeled previously (^{64}Cu-SarAr-ch14.18) and imaging verified selectivity for GD2-expressing human tumors grown subcutaneously in immunodeficient mice (*23*). We report here the evaluation of ^{64}Cu-*p*-NH_2-Bn-DOTA-hu14.18K322A in a similar mouse model. Imaging with the radiolabeled version of the same antibody used in treatment will provide insight into the ability of hu14.18K322A to reach its target, as well as insight into uptake in nontarget tissues that may cause side effects. Although all neuroblastoma tumors show some level of GD2 expression, a significant fraction of patients do not respond to therapy (*20*). Therefore, imaging using an anti-GD2 antibody could also provide measurement of GD2 expression levels in tumors and would thus be useful in identifying potential responders before the initiation of treatment.

MATERIALS AND METHODS

All chemicals were purchased from Sigma Chemical Co., unless otherwise noted. All solutions were prepared using deionized water (Milli-Q Integral Water Purification System [Millipore Corp.]; 18.2 MΩ·cm resistivity). Radioactive samples were analyzed in a CRC-15R dose calibrator (Capintec, Inc.) or a Wizard^2 3 automatic γ-counter (PerkinElmer Life and Analytic Sciences). Centrifugation was performed on a Sorvall Legend RT+ centrifuge (Thermo Scientific).

Cell Lines and Reagents

M21 melanoma cells were generously provided by Paul M. Sondel (University of Wisconsin-Madison). The M21 human melanoma line is a subclone derived in the laboratory of Dr. Ralph Reisfeld (Scripps Research Institute) from the human melanoma line UCLA-SO-M21, originally provided by Dr. Donald L. Morton (UCLA). Cells were grown in RPMI 1640 tissue culture medium (Invitrogen Corp. or Mediatech) supplemented with 10% fetal bovine serum (Invitrogen Corp. or Hyclone, Perbio Cell Culture Division) and L-glutamine (2 mM, Invitrogen Corp.). PC-3 (human metastatic prostate adenocarcinoma) cells were obtained from American Type Culture Collection and grown in F-12K medium (Invitrogen Corp.) with 10% fetal bovine serum. All cell lines were grown at 37°C in an atmosphere of 5% CO_2, as a semicontinuous adhesion culture with passaging by trypsinization every 3–4 d. Cells were used after 2 wk of initiation of culture and were grown in vitro for no longer than 12 wk.

Antibody Conjugation

The hu14.18K322A construct was provided by Merck KGaA, and the antibody was produced for clinical use by Children's GMP, LLC. The antibody solution was provided at a concentration of 8.6 mg/mL in phosphate-buffered saline (PBS), 100 mM arginine, and 0.03% polysorbate-80 at pH 6.0. Using the optimal method determined by previous studies (*24*), we accomplished conjugation with *p*-NH_2-Bn-DOTA (Macrocyclics) at a 500:1 molar excess in conjunction with *N*-(3-dimethylaminopropyl)-*N′*-ethylcarbodiimide in a 250:1 molar excess at pH 5 in 0.1 M sodium acetate for 30 min at 37°C. Unconjugated chelate was removed from the solution by high-performance liquid chromatography on an Agilent 1200 Series LC system (Agilent Technologies) monitored at 280 nm using a BioSEP SEC-S3000 size-exclusion column (Phenomenex) and a mobile phase of 100 mM sodium acetate, pH 5 (flow rate, 1.0 mL/min).

Radiolabeling with ^{64}Cu

^{64}Cu was produced at Washington University School of Medicine on a CS-15 biomedical cyclotron (*25*). A stock solution of ^{64}Cu in 0.05 M HCl was diluted in 0.1 M sodium acetate, pH 5.0, and 0.37–18.5 MBq (10–500 μCi) were added to a solution of 1–50 μg of *p*-NH_2-Bn-DOTA-hu14.18K322A and incubated for 30 min to 2 h at 25°C–40°C. Labeling efficiency was determined by radioactive thin-layer chromatography (radio-TLC) using instant TLC glass microfiber strips (Biodex) and analysis on an AR-2000 radio-TLC imaging scanner (Bioscan) using the WinScan 3 image analysis software. Radio-TLC plates of labeled antibodies were developed in 0.1 M sodium phosphate and 100 mM ethylenediaminetetraacetic acid (EDTA), pH 8, and compared with controls of ^{64}Cu alone and ^{64}Cu-EDTA. Once labeling was complete, 3 μL of 100 mM EDTA in 0.1 M sodium phosphate, pH 8, were added to the solution to scavenge any unbound copper. The unbound copper was then removed from the solution by passing it through a Microcon YM-30 filter (Millipore) via centrifugation at 14,000*g* for 15 min. Final pH was adjusted at this point if necessary, and radio-TLC was again performed to assess final radiochemical purity.

To determine the approximate number of chelates per antibody, isotopic dilution experiments were performed by following an adaptation of the method by Meares et al. (*26*). To 60 μL of 0.1 M

sodium acetate (pH 5.0), 10 μL of antibody solution (2 μg/mL) were added. A solution of copper chloride (100 mM) was mixed with a small amount of ^{64}Cu (~120 Bq or 3 μCi). Approximately 6.5 μL of this radioactive copper solution were added to the antibody solution and incubated for 1 h at 40°C. This addition results in a 3-times molar excess of copper to antibody. At the conclusion of the incubation, radio-TLC was performed to determine percentage labeling. A control radio-TLC (as above) of unbound copper confirmed that copper travels near the solvent front. Conversely, copper-labeled antibody does not move from the baseline. By multiplying percentage labeling by the known moles of copper added, one can determine the number of moles of copper that are bound. Using the equation reported (*26*), moles of bound copper are divided by the total moles of antibody to give a ratio of copper to antibody. Because each chelate can contain only 1 mol of copper, this results in a ratio of chelates per antibody.

Immunoreactivity

Gangliosides (GD2 or GD1b; EMD Biosciences, Inc.) were reconstituted in dimethylsulfoxide at a concentration of 1 mg/mL. Further dilutions of the gangliosides were performed with absolute ethanol. Microtiter plates (96-well, Immulon 4 HBX; Thermo Electron Corp.) were coated with 0.4 μg/well (100 μL) of GD2 or GD1b and allowed to dry at room temperature overnight with rotation (~70 rpm). Nonspecific sites were blocked for 1 h at room temperature with rotation (~70 rpm) using PBS containing 1.0% bovine serum albumin and 0.01% polysorbate-20. Plates were washed 3 times with PBS containing 0.05% polysorbate-20 on an ELx405 Select CW plate washer (Bio-Tek Instruments, Inc.). An aliquot of ^{64}Cu-*p*-NH_2-Bn-DOTA-hu14.18K322A was diluted in PBS containing 1.0% bovine serum albumin and added (93 kBq [2.5 μCi]/well) to various concentrations of hu14.18K322A (0–860 μg/well). The radiolabeled and cold antibody dilutions were mixed by gentle inversion, 100 μL of antibody solution were added to each well, and the plates were incubated at room temperature for 2 h with rotation (~70 rpm). Plates were then washed 3 times with the buffer stated previously, the wells were separated, and the radioactivity (counts per minute) in each well was determined with an automatic γ-counter. The previously determined ^{64}Cu counting efficiency of the γ-counter was used to convert to decays per minute (dpm) bound to each well. These data were decay-corrected, and all data points ($n = 4$ for each antibody concentration) were then plotted versus antibody concentration in micrograms per well. Fraction bound was calculated as the bound activity at each concentration divided by the activity bound in the absence of unlabeled antibody ([antibody] = 0 μg per well). Regression analysis was performed using the R software (version 2.13.1; R Foundation for Statistical Computing) with a binomial model, and this regression curve was used to quantify inhibition.

Cell Association Analysis

PC-3 and M21 cells were plated at 2×10^5 cells per well in 6-well plates (BD Falcon) 24 h before initiation of the study. Cells in half of the wells ($n = 3$) were blocked by incubation with 180 μg (10 μL) of unlabeled native antibody in 2 mL of medium. After 15 min, medium was removed and all wells were washed 3 times with 2 mL of PBS. A 0.11-MBq aliquot (3 μCi, ~0.5 μg) of ^{64}Cu-*p*-NH_2-Bn-DOTA-hu14.18K322A in 1.0 mL of medium was added to the cells and incubated at 37°C in a 5% CO_2 atmosphere. The blocked wells received an additional 180 μg (10 μL) of unlabeled native antibody to maintain antibody blocking throughout the experiment. Incubation was terminated at various times (5, 15, 30, or 60 min) by removing the radioactive culture medium, and the cells were washed 3 times with 2.0 mL of PBS. Cells were lysed and removed from the plate by the addition of 1.0 mL of 0.25% sodium dodecylsulfate. Radioactivity in the cell extracts, and a 0.111-MBq (3-μCi) dose standard, was measured in a γ-counter, and subsequently protein content was measured using a standard copper reduction–bicinchoninic acid assay (Pierce Biotechnology) with bovine serum albumin as the protein standard. Cell-associated radioactivity data for all experiments were normalized for the amount of protein in each sample. The percentage of cell-associated radioactivity was based on total radioactivity initially added to each well.

Tumor-Bearing Mice

All animal experiments were performed in compliance with Institutional Animal Care and Use Committee guidelines using approved protocols. Female athymic *nu/nu* mice, 2–3 mo of age and weighing 20–25 g, were purchased from Charles River Laboratories. For tumor implantation, cells were trypsinized (0.05% trypsin, 0.53 mM EDTA in Hanks balanced salt solution) and resuspended in sterile PBS at 4°C at a concentration of 5×10^7 cells per mL. The mice were anesthetized with isoflurane (2%–4% in a constant flow of oxygen) and injected subcutaneously in the rear flank with either M21 or PC-3 tumor cells (5×10^6/100 μL of sterile PBS). For the imaging studies, tumors were implanted bilaterally for direct comparison of tumor uptake within the same image. Tumors were allowed to grow to an average diameter of 7 mm (~3 wk).

Biodistribution of ^{64}Cu-*p*-NH_2-Bn-DOTA-hu14.18K322A

Tumor-bearing mice were injected retroorbitally (*27*), under 2% isoflurane, with 1.85–2.41 MBq (50–65 μCi) of ^{64}Cu-*p*-NH_2-Bn-DOTA-hu14.18K322A (100 μL). At 48 h after injection, the mice were sacrificed by decapitation under isoflurane (2%) anesthesia. Tissues were removed and weighed, and radioactivity was measured. Data were expressed as percentage of the injected dose per gram of tissue (wet weight) (%ID/g).

Small-Animal PET with ^{64}Cu-*p*-NH_2-Bn-DOTA-hu14.18K322A

Small-animal PET was performed on a Focus 120, and CT images were obtained using a microCAT II (both from Siemens Medical Solutions USA Inc.). AMIDE software (A Medical Imaging Data Examiner, http://amide.sourceforge.net/index.html) was used for image analysis. Statistical analysis (Student *t* test) was performed using Windows (Microsoft) Excel or GraphPad Prism (GraphPad Software).

For small-animal imaging studies, *p*-NH_2-Bn-DOTA-hu14.18K322A was labeled with ^{64}Cu supplied at 33.7 MBq/μL (0.91 mCi/μL) in 0.04 M HCl as described in the "Radiolabeling with ^{64}Cu" section. The radioimmunoconjugate was diluted with saline and sterile-filtered (0.2 μm) before injection. Animals were injected with ^{64}Cu-*p*-NH_2-Bn-DOTA-hu14.18K322A into the lateral tail vein (0.1 mL, 50 μg of antibody; mean activity, 5.2 MBq of ^{64}Cu [140 μCi; range, 135–145.5 μCi]). Mice were allowed to recover and given food and water ad libitum between imaging sessions. Isoflurane (2%–4%) was used as an inhaled anesthetic during imaging. Single-position, whole-body PET was performed at 1, 24, and 48 h after injection in 30-min static sessions. Images were reconstructed by 2-dimensional ordered-subset expectation maximization. At 48 h after injection, CT data were acquired. After CT, the mice were euthanized by CO_2 in-

halation, and a full biodistribution analysis was performed. Tissues were collected and weighed, and radioactivity was counted using an automated γ-counter. PET and CT images were registered manually using AMIDE software, and volumes of interest were drawn over tumor, lung, liver, kidney, brain, and muscle. Data from these volumes of interest were used to calculate biodistribution for each imaging session.

RESULTS

Preparation of ^{64}Cu-*p*-NH_2-Bn-DOTA-hu14.18K322A

The conjugation of the antibody with *p*-NH_2-Bn-DOTA at a 500:1 molar excess in conjunction with *N*-(3-dimethylaminopropyl)-*N′*-ethylcarbodiimide in a 250:1 molar excess at pH 5 in 0.1 M sodium acetate for 30 min at 37°C was successful. Isolation of the conjugated antibody was achieved by preparative high-performance liquid chromatography.

^{64}Cu-*p*-NH_2-Bn-DOTA-hu14.18K322A was prepared successfully at high radiochemical purity (≥95%). Optimal conditions for labeling were 30 min at 37°C and a ratio of 0.37 MBq/μg of antibody (10 μCi/μg of antibody) as confirmed by radio-TLC. Continued heating over several hours did not increase the radiolabeling yield. Specific activities, after purification, of 127–370 MBq/mg (3.4–10 mCi/mg) for the *p*-NH_2-Bn-DOTA complex were achieved. Isotopic dilution experiments over several batches of conjugated antibody estimated that there were 2.5–4.3 DOTA moieties per antibody.

Immunoreactivity

Before animal studies or cell-based assays, conservation of immunoreactivity was determined by measuring the binding of the conjugated antibody to purified GD2. Parallel assays used GD1b disialoganglioside as a negative control. These initial immunoreactivity studies demonstrated that ^{64}Cu-*p*-NH_2-Bn-DOTA-hu14.18K322A retained antigen binding to GD2, whereas binding to GD1b remained at background levels (Fig. 1). Furthermore, a dose-dependent inhibition of radiotracer binding was observed with increasing concentrations of unconjugated hu14.18K322A antibody (*log*[inhibitory concentration of 50%, or IC_{50}], −0.64 ± 0.22, corresponding to a dose of 0.23 μg/well or 14 nM). Inhibition of more than 95% of radiotracer binding was observed at doses above 3.3 μg/well (207 nM) of hu14.18K322A, and binding decreased to background levels at higher concentrations.

In Vitro Binding to GD2-Expressing Cells

Cell association of ^{64}Cu-*p*-NH_2-Bn-DOTA-hu14.18K322A was observed over 1 h in both M21 (GD2-positive) and PC-3 (GD2-negative) cells (Fig. 2). Uptake was 6-fold higher in the M21 cells (0.46%/mg of protein) when compared with the PC-3 cells (0.07%/mg of protein) after 60 min. Blocking with a 360-fold excess of unlabeled antibody decreased cell-associated radioactivity in both cell lines, with a larger effect seen in the M21 (~80% decrease) than in PC-3 (~20% decrease) cells. Taken together, these in vitro data indicate that specific binding of the antibody to GD2 was retained after the conjugation and labeling process.

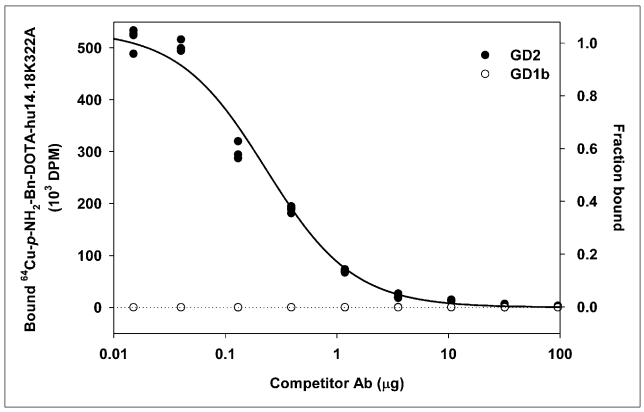

FIGURE 1. Concentration-dependent inhibition of ^{64}Cu-*p*-NH_2-Bn-DOTA-hu14.18K322A binding to GD2 and GD1b in presence of increasing concentrations of unmodified hu14.18K322A (*log* [IC_{50}] = −0.64 ± 0.22, corresponding to dose of 0.23 μg/well or 14 nM). Ab = antibody.

Biodistribution

In the biodistribution studies, athymic nude (*nu/nu*) mice bearing either PC-3 (GD2-negative) or M21 (GD2-positive) subcutaneous tumors were injected with ^{64}Cu-*p*-NH_2-Bn-DOTA-hu14.18K322A and sacrificed at various times after injection. As displayed in Table 1, the tracer concentration in all organs was significantly higher in the M21 tumor model than in the PC-3 tumor model, particularly with regard to tumor and blood. Even after 48 h, tracer concentration in the blood in the M21-bearing mice was 14.8% ± 1.3%, compared with 11.4% ± 0.5% for the PC-3–bearing mice (P = 0.0003). The tracer concentration was almost 2-fold higher in the M21 than in the PC-3 tumors (9.5% ± 2.6% vs. 5.0 ± 0.5 %ID/g, respectively; P = 0.0023). The uptake in the GD2-negative tumor is similar to that seen with other nonspecific labeled antibodies and is most likely due to the enhanced permeability and retention effect (*28*).

Tumor–to–nontarget tissue ratios clearly illustrate a significant difference in tracer uptake between the GD2-positive

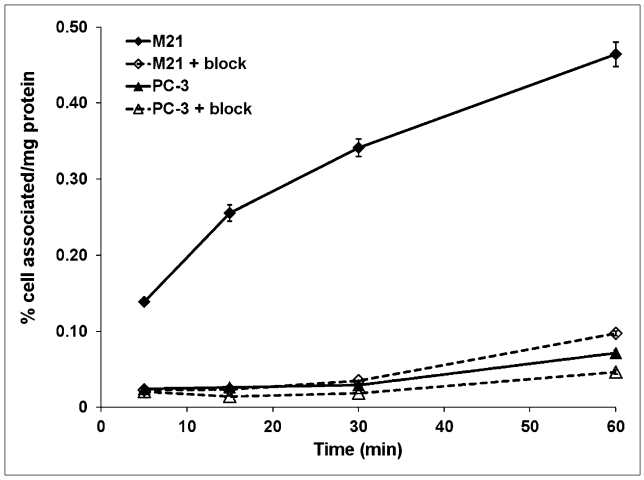

FIGURE 2. Cell association of ^{64}Cu-*p*-NH_2-Bn-DOTA-hu14.18K322A with M21 and PC-3 cell lines over 1 h of incubation. Data are normalized to mass of protein in sample.

TABLE 1
Biodistribution of ^{64}Cu-*p*-NH_2-Bn-DOTA-hu14.18K322A at 48 Hours After Injection

Tissue	%ID/g ± SD		
	M21 (n = 4)	PC-3 (n = 6)	P
Blood	14.79 ± 1.27	11.41 ± 0.50	0.0003
Liver	7.14 ± 0.70	5.58 ± 0.82	0.0146
Kidney	5.10 ± 0.29	4.59 ± 0.47	0.0925
Spleen	6.79 ± 1.66	4.55 ± 1.27	0.0411
Lung	9.93 ± 1.30	7.26 ± 1.39	0.0160
Heart	4.36 ± 0.70	3.27 ± 0.27	0.0078
Adrenal gland	4.91 ± 0.66	3.62 ± 0.49	0.0071
Bone (femur)	2.37 ± 0.22	1.79 ± 0.27	0.0073
Tumor	9.52 ± 2.55	4.96 ± 0.51	0.0023

P value calculated by 2-tailed, unpaired Student t test.

and -negative tumors (Fig. 3). For the M21 tumors, the tumor-to-organ ratios were 0.64 ± 0.18, 1.87 ± 0.51, and 1.33 ± 0.38 for blood (P = 0.025), kidney (P = 0.007), and liver (P = 0.031), respectively. In contrast, the ratios for the PC-3 tumors were 0.43 ± 0.05, 1.08 ± 0.16, and 0.89 ± 0.16 for blood, kidney, and liver, respectively, demonstrating nonspecific uptake.

Small-Animal PET with ^{64}Cu-*p*-NH_2-Bn-DOTA-hu14.18K322A

To assess efficacy as an imaging agent, ^{64}Cu-*p*-NH_2-Bn-DOTA-hu14.18K322A was injected via the tail vein into mice bearing bilateral tumors: 1 GD2-positive (M21) and 1 GD2-negative (PC-3). Single-position, whole-body PET was performed at 1, 24, and 48 h after injection, along with CT, after the 48-h PET session. In a representative image (Fig. 4), the M21 tumor is clearly seen whereas the PC-3 tumor is not. Furthermore, tracer concentration increases over time in the M21 tumor but not in the PC-3 tumor. In contrast, tracer uptake in the nontarget organs, such as the lung and liver, decreases with time (Fig. 5). For example, tracer concentration in the M21 tumor increased from 4.75 %ID per cubic centimeter (%ID/cm^3) at 24 h to 6.45 %ID/cm^3 at 48 h, and the corresponding values for the PC-3 tumor were 3.78 %ID/cm^3 and 3.67 %ID/cm^3.

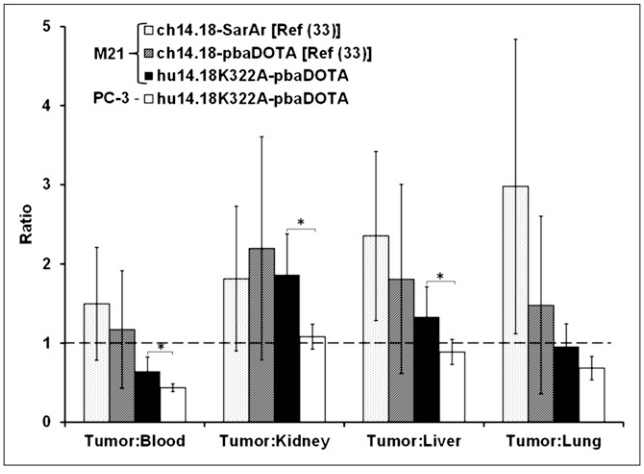

FIGURE 3. Comparison of tumor–to–nontarget tissue ratios of ^{64}Cu-*p*-NH_2-Bn-DOTA-hu14.18K322A to previously reported study with ^{64}Cu-*p*-NH_2-Bn-DOTA-ch14.18 and ^{64}Cu-*p*-NH_2-Bn-SarAr-ch14.18 (*33*) based on biodistribution data. *P < 0.05.

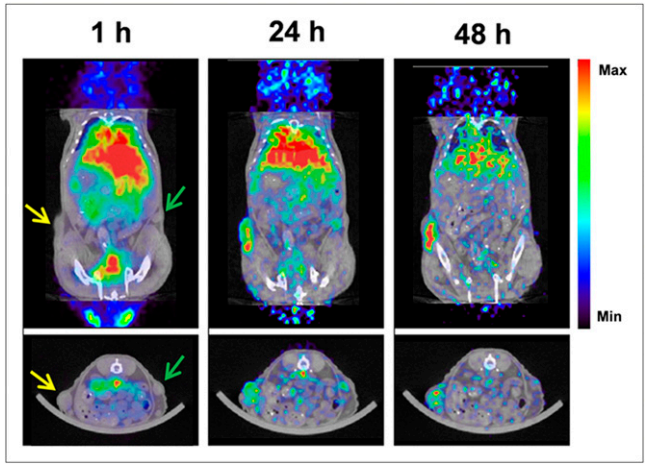

FIGURE 4. Representative small-animal PET images of athymic nude (*nu/nu*) mouse bearing M21 (yellow arrows) and PC-3 (green arrows) tumor implanted in flank and injected with approximately 5.2 MBq (140 μCi) of ^{64}Cu-*p*-NH_2-Bn-DOTA-hu14.18K322A.

DISCUSSION

Recently, Yu et al. showed that maintenance immunotherapy targeting GD2 increases 2-y event-free survival by 20% in neuroblastoma patients (*29*). The tumor-targeting ability of these antibodies and the immune response they elicit have been extensively studied (*19,29–31*). However, there has been little investigation of their retention in other organs (possibly related to the observed toxicity) or of the role of

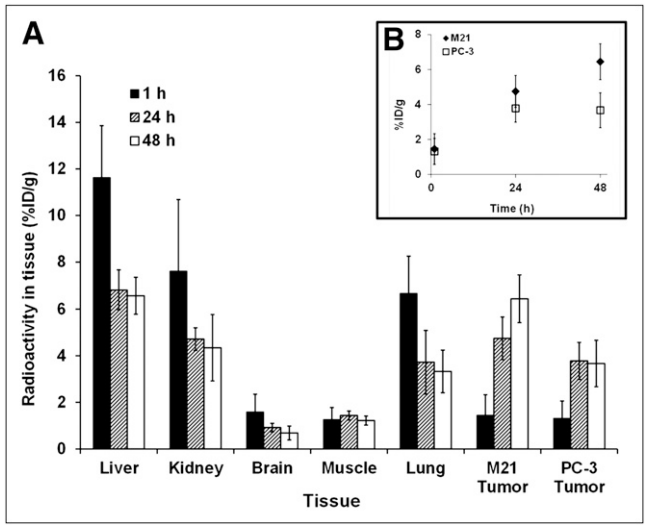

FIGURE 5. Tissue uptake data calculated from volume-of-interest analysis on small-animal PET images (n = 6) of *nu/nu* mice bearing bilateral PC-3 and M21 tumors injected with approximately 5.2 MBq (139 μCi) of ^{64}Cu-*p*-NH_2-Bn-DOTA-hu14.18K322A. (A) Direct comparison of M21 to PC-3 tumor uptake over time (B).

GD2 expression levels in patient response. Although imaging agents such as ^{123}I-metaiodobenzylguanidine are useful in detecting and monitoring the progression of neuroblastoma (*32*), they provide no direct information about antibody targeting or predicting patient response to immunotherapy.

In this study, we demonstrated that ^{64}Cu-labeled hu14.18K322A retains its antigen-binding ability after conjugation with chelators and radiolabeling as evidenced by the concentration-dependent binding of ^{64}Cu-*p*-NH_2-Bn-DOTA-hu14.18K322A to purified GD2 with minimal binding to GD1b (>1,000-fold lower binding to GD1b than GD2). This binding was also demonstrated by the 6-fold-higher cell association of the tracer with the GD2-positive tumor cells (M21) than with the GD2-negative tumor cells (PC-3).

In vivo radiotracer quantification using both dissection and small-animal PET was performed in immunodeficient mice bearing subcutaneous human M21 and PC-3 tumors. Although less rigorous than spontaneously arising or orthotopic tumor models because of the altered microenvironment, these subcutaneous implants provide an efficient and well-accepted model for the initial evaluation of radiotracers (*23,33–35*). It is also possible that the binding and clearance of this humanized antibody may differ significantly between our immunodeficient mouse model and human patients. However, several humanized antibodies have been explored in mouse models of disease and translated successfully into human trials, including radiolabeled versions of trastuzumab (Herceptin; Genentech) and bevacizumab (Avastin; Genentech). Hundreds more have been assessed as radiolabeled agents, and a comprehensive summary can be found in the Molecular Imaging and Contrast Agent Database (www.ncbi.nlm.nih.gov/books/NBK5330/).

The biodistribution data for ^{64}Cu-*p*-NH_2-Bn-DOTA-hu14.18K322A were consistent with the corresponding ^{64}Cu-*p*-NH_2-Bn-DOTA-ch14.18 data (*33*). In the biodistribution study, a nearly 2-fold-higher tumor uptake in M21 than PC-3 tumors was observed, once again demonstrating the affinity for GD2-positive over GD2-negative tumors. Likewise, the small-animal PET data showed an increase in tumor uptake over time in the M21 tumor whereas the PC-3 tumor had a low tracer uptake throughout the study. The antigen-binding region is retained between ch14.18 and hu14.18K322A, and thus both should recognize GD2 equally well. Binding equivalence between these 2 antibodies is supported by the tumor-to-nontarget ratios shown in Figure 3. No statistically significant differences were seen in the M21 tumor-to-nontarget ratios for ^{64}Cu-*p*-NH_2-Bn-DOTA-hu14.18K322A, compared with the corresponding ch14.18 chelate (33). Significance was observed only for M21, compared with PC-3, tumor-to-nontarget ratios. The SarAr conjugate also did not show statistically significant improvement in tumor-to-nontarget ratios as may be expected with this more stable chelate. Another confounding factor with SarAr is the lack of human data for this chelator. The ultimate goal of this project is the rapid translation of labeled hu14.18K322A radiotracers into the clinic, and SarAr conjugation would impart the need for additional experiments to establish safety for human use. This added time and expense are not adequately justified by the modest improvement in tumor-to-nontarget ratios.

In contrast to the substantial decline in tracer activity in nontumor tissues between 24 and 48 h, no significant change in uptake or clearance of any organs between 48 and 72 h was observed (all P values > 0.1, data not shown). Although data at 72 h showed little difference from the 48-h data, much longer time points may. Recent work has demonstrated the use of ^{89}Zr, with its 3.27-d half-life and favorable positron energies, chelated to an antibody for imaging, and these ^{89}Zr chelates have shown excellent images out to 144 h (*34*).

As was observed for the ch14.18 conjugates in similar humanized mouse models of melanoma (*33*), significant nontarget uptake was also evident with ^{64}Cu-*p*-NH_2-Bn-DOTA-hu14.18K322A. In the present study, the biodistribution experiment showed 7 %ID/g uptake in the liver and 5 %ID/g uptake in the kidney after 48 h, which is most likely due to minimal copper loss or metabolism of the construct. The dissociation of copper from macrocyclic chelators will occur to some degree, and it has been demonstrated that in the liver, copper is transchelated by proteins, especially superoxide dismutase (*36,37*). In the kidney, conversion of copper radiopharmaceuticals to low-molecular-weight metabolites has been observed (*38*).

In addition to the release of copper from the chelator or metabolism, there is the possibility of GD2-positive cells present outside the primary tumor site that could also bind the tracer. Radioactivity accumulation in all nontarget organs (Table 1) was higher in M21 than PC-3 groups, particularly blood, which was nearly 30% higher ($P = 0.0003$) at 48 h after injection in M21-bearing mice (14.8% ± 1.3% vs. 11.4% ± 0.5% in PC-3 mice). Slow clearance of radioactivity from the blood is not uncommon for radiotracers based on full-length monoclonal antibodies (*35*) and accounts for the high blood radioactivity levels in both M21 and PC-3 tumor–bearing animals. These data are also consistent with the ch14.18-based radiotracers (*33*). The prolonged residence of unbound antibody in the blood could affect dosimetry or tumor visualization by increasing radiotracer delivery to nontarget tissues. However, the continued clearance from blood and all other organs over time, as seen in the small-animal PET data, allows for easy delineation of the tumor at later time points.

Slow antibody clearance does not account for the difference in blood radioactivity levels between the M21 and PC-3 animals. A clinical analysis of patients with all stages of neuroblastoma demonstrated the presence of GD2 in the sera of all patients above stage II at levels 3–50 times greater than stages I–II or healthy children (*39*). Thus, the discrepancy between blood levels in the M21 and PC-3 tumor–bearing mice may be attributed to this phenomenon, and these high blood levels may also contribute to the higher levels of radioactivity measured in other blood-bearing tissues, such as the lung, heart and spleen, and in femur bone, which included marrow.

CONCLUSION

^{64}Cu-*p*-NH_2-Bn-DOTA-hu14.18K322A is a novel PET radiotracer that may facilitate clinical investigations of neu-

roblastoma immunotherapies and thus complement other imaging modalities in the staging and treatment of neuroblastoma. Preliminary in vitro and in vivo data confirm specificity of binding to GD2 and significant GD2-positive tumor-targeting ability. With further study, this tracer may allow patient screening protocols to be developed, thus maximizing the clinical impact of anti-GD2 immunotherapy by targeting those patients most likely to benefit from a GD2-targeted therapy regimen.

DISCLOSURE STATEMENT

The costs of publication of this article were defrayed in part by the payment of page charges. Therefore, and solely to indicate this fact, this article is hereby marked "advertisement" in accordance with 18 USC section 1734.

ACKNOWLEDGMENTS

We thank Sandra Gaither for her assistance with manuscript preparation and Dr. Robert Ogg for his assistance with statistical analysis. We also thank Tracy McGraw and Elizabeth Shy for their assistance with the in vitro and in vivo studies. The production of ^{64}Cu at Washington University School of Medicine was supported by NCI Radionuclide Resource for Cancer Applications grant R24 CA86307. Research funding was provided by ALSAC–St. Jude Children's Research Hospital and the Children's Hospital (Boston) Radiology Foundation. No other potential conflict of interest relevant to this article was reported.

REFERENCES

1. Sharp SE, Gelfand MJ, Shulkin BL. Pediatrics: diagnosis of neuroblastoma. *Semin Nucl Med.* 2011;41:345–353.
2. Brodeur GM. Neuroblastoma: biological insights into a clinical enigma. *Nat Rev Cancer.* 2003;3:203–216.
3. Kushner BH. Neuroblastoma: a disease requiring a multitude of imaging studies. *J Nucl Med.* 2004;45:1172–1188.
4. Jemal A, Siegel R, Ward E, Hao Y, Xu J, Thun MJ. Cancer statistics, 2009. *CA Cancer J Clin.* 2009;59:225–249.
5. Cheung NK, Lazarus H, Miraldi FD, et al. Ganglioside GD2 specific monoclonal antibody 3F8: a phase I study in patients with neuroblastoma and malignant melanoma. *J Clin Oncol.* 1987;5:1430–1440.
6. Choi BS, Sondel PM, Hank JA, et al. Phase I trial of combined treatment with ch14.18 and R24 monoclonal antibodies and interleukin-2 for patients with melanoma or sarcoma. *Cancer Immunol Immunother.* 2006;55:761–774.
7. Albertini MR, Hank JA, Schiller JH, et al. Phase IB trial of chimeric antidisialoganglioside antibody plus interleukin 2 for melanoma patients. *Clin Cancer Res.* 1997;3:1277–1288.
8. Murray JL, Kleinerman ES, Jia SF, et al. Phase Ia/Ib trial of anti-GD2 chimeric monoclonal antibody 14.18 (ch14.18) and recombinant human granulocyte-macrophage colony-stimulating factor (rhGM-CSF) in metastatic melanoma. *J Immunother Emphasis Tumor Immunol.* 1996;19:206–217.
9. Saleh MN, Khazaeli MB, Wheeler RH, et al. Phase I trial of the chimeric anti-GD2 monoclonal antibody ch14.18 in patients with malignant melanoma. *Hum Antibodies Hybridomas.* 1992;3:19–24.
10. Yu AL, Uttenreuther-Fischer MM, Huang CS, et al. Phase I trial of a human-mouse chimeric anti-disialoganglioside monoclonal antibody ch14.18 in patients with refractory neuroblastoma and osteosarcoma. *J Clin Oncol.* 1998;16:2169–2180.
11. Gilman AL, Ozkaynak MF, Matthay KK, et al. Phase I study of ch14.18 with granulocyte-macrophage colony-stimulating factor and interleukin-2 in children with neuroblastoma after autologous bone marrow transplantation or stem-cell rescue: a report from the Children's Oncology Group. *J Clin Oncol.* 2009;27:85–91.
12. Handgretinger R, Anderson K, Lang P, et al. A phase I study of human/mouse chimeric antiganglioside GD2 antibody ch14.18 in patients with neuroblastoma. *Eur J Cancer.* 1995;31A:261–267.
13. Ozkaynak MF, Sondel PM, Krailo MD, et al. Phase I study of chimeric human/murine anti-ganglioside G(D2) monoclonal antibody (ch14.18) with granulocyte-macrophage colony-stimulating factor in children with neuroblastoma immediately after hematopoietic stem-cell transplantation: a Children's Cancer Group Study. *J Clin Oncol.* 2000;18:4077–4085.
14. Modak S, Cheung NK. Disialoganglioside directed immunotherapy of neuroblastoma. *Cancer Invest.* 2007;25:67–77.
15. Cheresh DA, Harper JR, Schulz G, Reisfeld RA. Localization of the gangliosides GD2 and GD3 in adhesion plaques and on the surface of human melanoma cells. *Proc Natl Acad Sci USA.* 1984;81:5767–5771.
16. Saito M, Yu RK, Cheung NK. Ganglioside GD2 specificity of monoclonal antibodies to human neuroblastoma cell. *Biochem Biophys Res Commun.* 1985;127:1–7.
17. Saarinen UM, Coccia PF, Gerson SL, Pelley R, Cheung NK. Eradication of neuroblastoma cells in vitro by monoclonal antibody and human complement: method for purging autologous bone marrow. *Cancer Res.* 1985;45:5969–5975.
18. Mueller BM, Reisfeld RA, Gillies SD. Serum half-life and tumor localization of a chimeric antibody deleted of the CH2 domain and directed against the disialoganglioside GD2. *Proc Natl Acad Sci USA.* 1990;87:5702–5705.
19. Barker E, Mueller BM, Handgretinger R, Herter M, Yu AL, Reisfeld RA. Effect of a chimeric anti-ganglioside GD2 antibody on cell-mediated lysis of human neuroblastoma cells. *Cancer Res.* 1991;51:144–149.
20. Yu AL, Gilman AL, Ozkaynak MF, et al. Anti-GD2 antibody with GM-CSF, interleukin-2, and isotretinoin for neuroblastoma. *N Engl J Med.* 2010;363:1324–1334.
21. Sorkin LS, Otto M, Baldwin WM 3rd, et al. Anti-GD(2) with an FC point mutation reduces complement fixation and decreases antibody-induced allodynia. *Pain.* 2010;149:135–142.
22. Navid F, Barfield RC, Handgretinger R, et al. A novel anti-GD2 monoclonal antibody (mAb), hu14.18K322A, in children with refractory or recurrent neuroblastoma: early-phase evaluation [abstract]. *J Clin Oncol.* 2011;29(15 suppl):9523.
23. Voss SD, Smith SV, DiBartolo N, et al. Positron emission tomography (PET) imaging of neuroblastoma and melanoma with ^{64}Cu-SarAr immunoconjugates. *Proc Natl Acad Sci USA.* 2007;104:17489–17493.
24. Vavere AL, Dearling JL, Packard AB, et al. Chelate conjugation and Cu-64 labeling of Hu14.18K322A, an antibody targeting neuroblastoma. *J Labelled Comp Radiopharm.* 2009;52(suppl 1):S405.
25. McCarthy DW, Shefer RE, Klinkowstein RE, et al. Efficient production of high specific activity ^{64}Cu using a biomedical cyclotron. *Nucl Med Biol.* 1997;24:35–43.
26. Meares CF, McCall MJ, Reardan DT, Goodwin DA, Diamanti CI, McTigue M. Conjugation of antibodies with bifunctional chelating agents: isothiocyanate and bromoacetamide reagents, methods of analysis, and subsequent addition of metal ions. *Anal Biochem.* 1984;142:68–78.
27. Price JE, Barth RF, Johnson CW, Staubus AE. Injection of cells and monoclonal antibodies into mice: comparison of tail vein and retroorbital routes. *Proc Soc Exp Biol Med.* 1984;177:347–353.
28. Maeda H. Tumor-selective delivery of macromolecular drugs via the EPR effect: background and future prospects. *Bioconjug Chem.* 2010;21:797–802.
29. Navid F, Santana VM, Barfield RC. Anti-GD2 antibody therapy for GD2-expressing tumors. *Curr Cancer Drug Targets.* 2010;10:200–209.
30. Kowalczyk A, Gil M, Horwacik I, Odrowaz Z, Kozbor D, Rokita H. The GD2-specific 14G2a monoclonal antibody induces apoptosis and enhances cytotoxicity of chemotherapeutic drugs in IMR-32 human neuroblastoma cells. *Cancer Lett.* 2009;281:171–182.
31. Navid F, Armstrong M, Barfield RC. Immune therapies for neuroblastoma. *Cancer Biol Ther.* 2009;8:874–882.
32. Sharp SE, Shulkin BL, Gelfand MJ, Salisbury S, Furman WL. ^{123}I-MIBG scintigraphy and ^{18}F-FDG PET in neuroblastoma. *J Nucl Med.* 2009;50:1237–1243.
33. Dearling JL, Voss SD, Dunning P, et al. Imaging cancer using PET- the effect of the bifunctional chelator on the biodistribution of a ^{64}Cu-labeled antibody. *Nucl Med Biol.* 2011;38:29–38.
34. Holland JP, Divilov V, Bander NH, Smith-Jones PM, Larson SM, Lewis JS. ^{89}Zr-DFO-J591 for immunoPET of prostate-specific membrane antigen expression in vivo. *J Nucl Med.* 2010;51:1293–1300.
35. Lewis MR, Wang M, Axworthy DB, et al. In vivo evaluation of pretargeted ^{64}Cu for tumor imaging and therapy. *J Nucl Med.* 2003;44:1284–1292.
36. Bass LA, Wang M, Welch MJ, Anderson CJ. In vivo transchelation of copper-64 from TETA-octreotide to superoxide dismutase in rat liver. *Bioconjug Chem.* 2000;11:527–532.
37. Boswell CA, Sun X, Niu W, et al. Comparative in vivo stability of copper-64-labeled cross-bridged and conventional tetraazamacrocyclic complexes. *J Med Chem.* 2004;47:1465–1474.
38. Rogers BE, Anderson CJ, Connett JM, et al. Comparison of four bifunctional chelates for radiolabeling monoclonal antibodies with copper radioisotopes: biodistribution and metabolism. *Bioconjug Chem.* 1996;7:511–522.
39. Schulz G, Cheresh DA, Varki NM, Yu A, Staffileno LK, Reisfeld RA. Detection of ganglioside GD2 in tumor tissues and sera of neuroblastoma patients. *Cancer Res.* 1984;44:5914–5920.